Growth and local electronic properties of Cobalt nanodots underneath graphene on SiC(0001)

Yann Girard, Sarah Benbouabdellah, Outhmane Chahib, Cyril Chacon, Amandine Bellec, Vincent Repain, Jérôme Lagoute, Yannick Dappe, César González, Wei-Bin Su

Graphical Abstract

Growth and local electronic properties of Cobalt nanodots underneath graphene on SiC(0001)

Yann Girard, Sarah Benbouabdellah, Outhmane Chahib, Cyril Chacon, Amandine Bellec, Vincent Repain, Jérôme Lagoute, Yannick J. Dappe, César González, Wei-Bin Su

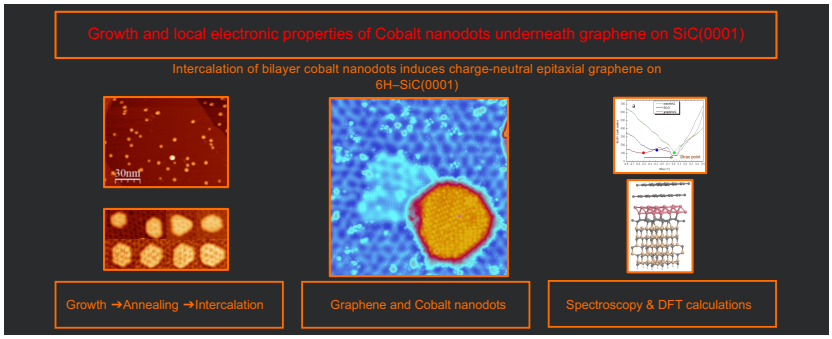

Growth and local electronic properties of Cobalt nanodots underneath graphene on SiC(0001)

Yann Girard[a,*], Sarah Benbouabdellah[a], Outhmane Chahib[a], Cyril Chacon[a], Amandine Bellec[a], Vincent Repain[a], Jérôme Lagoute[a], Yannick J. Dappe[b], César González[c], Wei-Bin Su[d]

[a] *Université Paris Cité, CNRS-UMR7162, Laboratoire Matériaux et Phénomènes Quantiques (MPQ), 75013 Paris, France*
[b] *SPEC, CEA, CNRS, Université Paris-Saclay, CEA Saclay 91191 Gif-sur-Yvette Cedex, France*
[c] *Departamento de Física de Materiales, Universidad Complutense de Madrid, E-28040 Madrid, Spain*
[d] *Institute of Physics, Academia Sinica, Nankang, Taipei 11529, Taiwan*

Abstract

The coupling of graphene with a ferromagnetic material opens opportunities for technological innovations in spintronics. To obtain this coupling it is necessary to control the elaboration of interfaces at the atomic scale. Here, we present results on cobalt intercalation between graphene and a buffer layer supported on a SiC(0001) substrate. As a result, we obtain cobalt islands covered by graphene whose local electronic properties are measured by scanning tunnelling microscopy and spectroscopy. These islands reveal two very distinct shapes and properties. Small-islands with atomic height and very narrow size distribution and, more interestingly, flat cobalt nanodots lower than one nanometer high, that are encapsulated by graphene. Compared to a graphene monolayer on SiC, those nanodots exhibit very different spectroscopic signatures. Using dI/dV local differential conductance spectra together with an analysis of image potential surface states measured thanks to dz/dV spectra, we show that graphene on the nanodots is neutrally charged. Moreover, its 4.65 eV work function is surprisingly larger than the predicted value of 3.8 eV for graphene on Co. First principle calculations show that those Co nanodots can be seen as cobalt bilayer sandwiched between two carbon planes.

Keywords: Graphene, Cobalt, Silicon Carbide, Field effect resonance, Scanning tunnelling microscopy / spectroscopy, Density Functional Theory calculations

1. Introduction

Graphene in contact with metallic surfaces presents specific electronic and magnetic properties depending on the coupling strength. This coupling ranges from weak

*Corresponding author
Email address: yann.girard@u-paris.fr (Yann Girard)

van der Waals interaction, leading to small doping, to a strong hybridization with its support, or functionalized molecules, leading to a drastic modification of its intrinsic properties. For example by the disappearance of its π orbitals [1, 2]. In the case of magnetism induced in π orbitals by proximity effects with a ferromagnetic element [3] or a topological insulator [4], the quality of the interfaces is essential [5]. Regarding doping by proximity effect, it is important to control the position of the Dirac Point (DP) relative to the Fermi Level (FL), for example, to create new quantum states when the neutrality point is obtained [6, 7] or to change the orientation of the spin current in spin-valves [8].

However, it is interesting to go beyond 2D systems and to study 1D or even 0D systems. We already know how to fabricate graphene nanoflakes or nanowires which also present surprising properties essentially linked to their edges or confinement effects. It is then interesting to study and compare the properties of these reduced graphene pieces to the ones of a full graphene plane by proximity with cobalt, for example, those of graphene flakes on Co(0001) [9, 10]. Here, we are interested in the encapsulation of cobalt (Co) nanodots (0D) between two carbon (C) planes (2D) supported on a silicon carbide sample, SiC(0001). The experiments previously performed on the system (graphene, Co, SiC) have either focused on Co ultra-thin films, leading to intercalated aggregates/clusters/atoms [11, 12, 13, 14, 15, 16], or on Co thin films (1 to 10 nm) intercalated below a graphene plane and directly in contact with the SiC substrate, forming cobalt silicides [17, 18]. Here, we present results of cobalt intercalation of an average thickness (before annealing) around one equivalent Co monolayer (1 Co ML = 18 10^{14} Co/cm^2) sandwiched between graphene and the buffer layer (BL) after annealing. The choice of this substrate is motivated by the fact that SiC(0001) is ideal to obtain graphene with a rather well-controlled thickness because it does not require any transfer. Moreover, SiC is a semiconductor and the final system is therefore quite useful for electronic devices.

It is now well established that confined growth [19, 20, 21] using this matrix, graphene on SiC, leads to spectacular effects for a wide diversity of intercalated species such as 2D gold, which becomes a semiconductor [22], calcium C_6CaC_6, which exhibits superconductivity at 4 K [23, 24], tin which drives graphene to its charge neutrality point [6] etc. and of course, Co [15, 16, 25, 18]. However, one has to consider two starting confining matrices. On one side, a BL on the SiC substrate (also called zero layer graphene or ZLG which can be transformed into monolayer graphene thanks to various intercalated species) with more or less regularly spaced sp^3 bonds between C and Si atoms exhibiting a $(6\sqrt{3}\times 6\sqrt{3})R30^\circ$ superstructure [26, 27]. On the other side, a graphene layer (or bilayer) on this BL. Concerning Co intercalation, final properties must be drastically different in these two situations, and we present here new results in the case of this second type of matrix.

In the following, we will show how to obtain graphene-encapsulated Co nanodots in three steps, the whole being performed *in situ* under Ultra-High Vacuum (UHV). i) Formation of monolayer and bilayer graphene (MLG and BLG) on a carbon BL by direct-heating of a clean SiC(0001) substrate, ii) formation of Co 3D islands at room temperature (RT) by evaporation of Co atoms and, finally, iii) production of graphene-covered nanodots by post-annealing at high temperature. Each of these steps is controlled by Scanning Tunneling Microscopy (STM) image analysis and the related local

electronic properties are obtained by Scanning Tunneling Spectroscopy (STS). Note also that we compared the doping, *i.e.* the DP position relatively to the Fermi level measured by STS once Co has been intercalated, to first principle calculations based on Density Functional Theory (DFT) performed on the pristine graphene band structure as a function of the number of graphene layers above a BL on SiC. This comparison has allowed us to discuss the effect of Co intercalation on graphene electronic properties.

2. Methods

2.1. ***Sample preparation***

The graphene synthesis is performed in a first UHV chamber (base pressure 7.10^{-10} mbar), the so-called synthesis chamber in the following, equipped with a Low Energy Electron Diffraction/Auger Electron Spectroscopy (LEED/AES) set-up (four grids Spectaleed) and a Variable Temperature STM (Omicron VT-STM). The SiC samples (10 mm $\times$ 5 mm $\times$ 0.3 mm, purchased from NOVASIC (France), silicon face epiready) are cleaned with alcohol / acetone / distilled water and degassed overnight under UHV at 750 °C (direct current heating, the temperature is measured by an IGA 5 pyrometer working in the spectral range 1.45 to 1.8 micrometers with an emissivity of 0.90). Then, the last traces of oxides observed by AES (electron primary energy of 1.5 or 2.5 keV, modulation of 10 V rms at 1 kHz and time constants of 300 msec were used in the phase-sensitive detector) are removed by exposing the surface to a silicon flux (Si flakes in a carbon crucible heated by an EFM 300 electron beam evaporator, the typical Si flux at the flux monitor stage is around 50 nA). Next, SiC samples are heated very quickly to 1400-1450 °C for one minute by direct heating (pressure stays lower than 5.10^{-8} mbar during this heating) and then thermalized in a few minutes once the current has been switched off. The Co is evaporated at room temperature on these samples thanks to a second electron beam evaporator where a Co rod is heated by electron bombardment (1 kV, electron emission around a few tenths of mA, ion flux around 20 nA). Typical deposition flux (see Supplementary file Appendix A) is about 0.15 ±0.05 ML per minute, calibrated by Co deposition on an Au(111) surface. We then check the surface cleanliness by STM at RT. Co intercalation is obtained by post-annealing for a few minutes (see below) at 900-950 °C.

2.2. ***STM/STS measurements***

All the atomic resolution STM images and STS measurements (dI/dV and dz/dV) have been performed in a second UHV chamber (base pressure around 5.10^{-11} mbar) equipped with an OMICRON Low-Temperature STM (4 K). The samples prepared in the synthesis chamber are transferred into the second one (the so-called measurements chamber in the following text), a few days after their synthesis and degassed for 10 minutes between 300 °C and 600 °C to remove water adsorption (the samples were kept in an air atmosphere). Before STS, STM tips are prepared on an Au(111) surface until the Au Shockley state is observed. Moreover, we have checked regularly that the pseudo-gap phonon of the graphene is observed near the Fermi Level. STM images are processed by WSXM [55].

2.3. *First-principles calculations*

Density Functional Theory calculations have been performed in order to follow the evolution of the Dirac point position as a function of the number of graphene layers and to calculate the density of states of various atomic configurations presented in Sec. 3.4. We used the very efficient DFT localized orbital Fireball code [63]. This code uses a self-consistent version of the Harris-Foulke LDA functional [53, 48] and the self-consistency is achieved over the occupation numbers. Optimized numerical basis sets have been used for cobalt, carbon, silicon and hydrogen with respective cutoff radii in atomic units of s = 6.5, p = 6.5,d = 6.5 for Co, s = 4.5, p = 4.5 for C, s = 4.8, p = 5.4 for Si, and s = 4.1 for H [30]. The Fireball code has been used to optimize the different structures considered in this work. All the calculated configurations have been optimized until the forces were below 0.1 eV/Å. The inter-layer distance has been determined using the so-called LCAO-S^2 + van der Waals formalism [42]. This procedure and basis set have already been used successfully in good agreement with similar experimental determinations [41, 43, 72]. Once the equilibrium configuration is found, the electronic structure of each configuration has been analyzed by means of band structure and DOS calculations. A set of 300 specific k-points along the Γ-K-M path has been used for band structure calculations.

3. Results and Discussion

3.1. *Growth of Co islands on graphene on SiC(0001)*

At first, it is important to verify that the Cobalt atoms are evaporated on a graphene monolayer fully covering the BL on SiC and not on a mix of graphene and BL. As such, several possibilities were available based on previous STM studies. i) Measurement of step edge heights before Co evaporation [47], (ii) identification of BL and MLG regions as a function of the density of cobalt islands formed at RT, (much higher on BL) [12], (iii) atomic corrugations of BL, MLG and BLG [38, 68]. Since our goal is the intercalation of Co between the BL and graphene, it turns out that (ii) is the most appropriate as detailed in Supplementary file Appendix A in Figures A.1 to A.4.

3.2. *Cobalt intercalation between graphene and buffer layer*

Once a Co sub-monolayer has been deposited at RT on graphene (see Supplementary file Appendix A), we anneal it in the synthesis chamber for five to ten minutes at 900 – 1000 °C. Fig. 1a. shows a large-scale STM image where two different features are circled, small protrusions that we call small-islands (size around 2-10 nm, height 2.6 ± 0.1Å, see a zoom in Fig. 1b), and bigger ones called nanodots (size around 10-50 nm, height between 3.5 to 9 Å, see Fig. 1c). The very rare Co islands of a few nm in height (saturated in the image) are remnants of the islands formed at RT that have not been completely evaporated. The remaining parts of the surface are covered with a graphene layer covering various underlying SiC terraces. The heights of these terraces are reminiscences of the 2.5 Å distance separating two consecutive SiC bi-layers of the 4-H SiC bulk. Previous X-ray Photoemission Spectroscopy (XPS) measurements have clearly shown that starting from an ultrathin film of as-deposited Co atoms at RT on

a SiC/BL/MLG, there is no Co intercalation below the BL for this range of temperatures [11, 25]. Here, we used this template and therefore Co atoms are necessarily embedded between the graphene and the BL. This is important and very different from previous observations of Fe [67], Co [18] or Pb [88] intercalation underneath the BL where these elements are connected to underlying Si dangling bonds, which leads to the transformation of the BL into MLG.

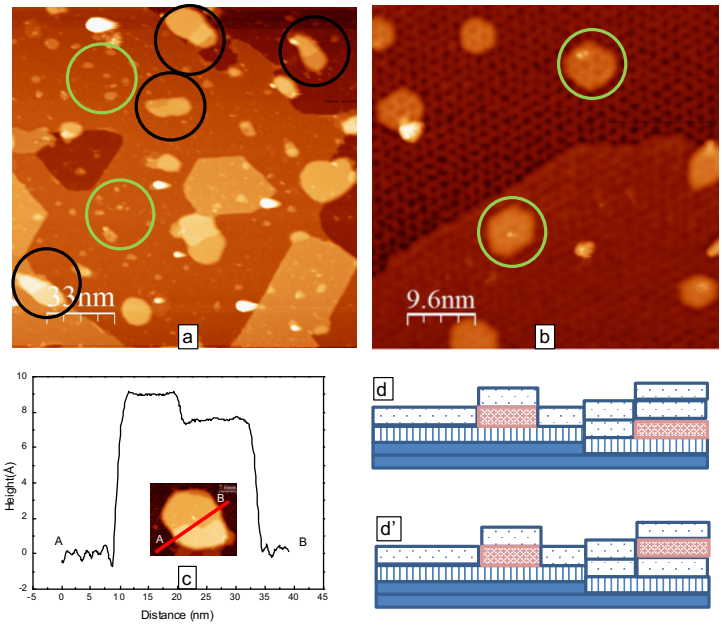

Figure 1: a) Scanning Tunneling Microscopy (STM) image of Co/graphene after 10 minutes annealing at 900 °C (160x160 nm^2, -2 V, 3 pA). b) Zoom of typical areas circled in green in a) showing the first kind of Co clusters intercalated under graphene called latter small-islands (50x50 nm^2, -3 V, 3 pA). The very different contrasts between the upper and lower halves of the image are attributed to monolayer and bilayer graphene (MLG and BLG). c) Height profile along the AB line in the inset showing a STM image (38x32 nm^2, -2 V, 5 pA) of a typical Co nanodot circled in black in a). d) and d'), sketches of two possible topological interpretations of b): red-dotted rectangles correspond to embedded Co atoms below graphene, dark-blue to SiC terraces, dotted rectangles to the graphene, dashed rectangle to the buffer layer (BL).

3.2.1. Cobalt clusters intercalated under graphene: small-islands

We will show that the small-islands visible in Fig. 1b on the upper (resp. lower) part of the image are located under a MLG (resp.BLG) and are similar to the ones that have already been observed by STM [16]. Their nearly hexagonal shape associated with a clear atomic or electronic corrugation is very different from previously observed embedded clusters obtained through a complex oxidation/deoxidation procedure of Co intercalation below the BL [15]. Nevertheless, concerning the intercalation within a BLG, it is not obvious at this stage, without atomic resolution and local spectroscopy measurements, to discriminate Co intercalation below a BLG or sandwiched between

two MLG, as shown in Figs. 1d and 1d'. However, we can definitively rule out the intercalation below the BL as already said before concerning the annealing temperature and as shown in Fig. 2. This image is the derivative of the right-handed inset. Small-islands are clearly seen on three terraces separated by 2.5 Å. We note that the expected large corrugation for BL areas compared to graphene areas (see also Supplementary file Fig. A.1) that should be amplified in this derived image is completely absent [68, 78]. The largest part of this area is covered by BLG and on the terrace on the left side, the slightly higher corrugation corresponds to MLG. If we compare a zoom on that BLG area as reported in Fig. 3a and the previous one in Fig. 1b, we can notice that Co clusters embedded in a MLG present a greater contrast compared to clusters embedded in BLG. Consequently, we can deduce that Co clusters are necessarily located between the BL and one or two graphene layers. Also, the more or less pronounced contrast corresponds to the signature of the number of graphene layers. Note that for all the synthesis processes used, we have never succeeded in increasing their lateral size beyond a few nanometers. Moreover, these nano-islands have no specific electronic signature compared to BLG (see below). We still do not know the configurations of the Co atoms (if any) under these small bumps.

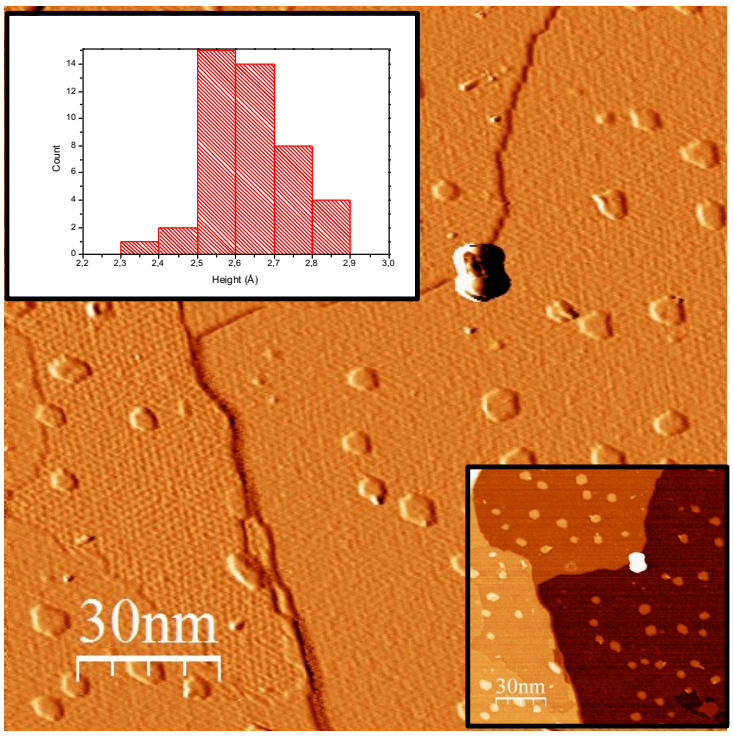

Figure 2: Derived STM image of the right inset showing an ensemble of small-islands corresponding to an area of Co intercalated graphene exempted of Co nanodots (150x150 nm^2, -1.4 V, 5 pA). Notice the different roughnesses of the right area and of the left terrace, this difference is a typical signature of BLG which here covered the majority of the surface. The left inset shows a height histogram of small-islands, the average height is 2.6 ± 0.1Å).

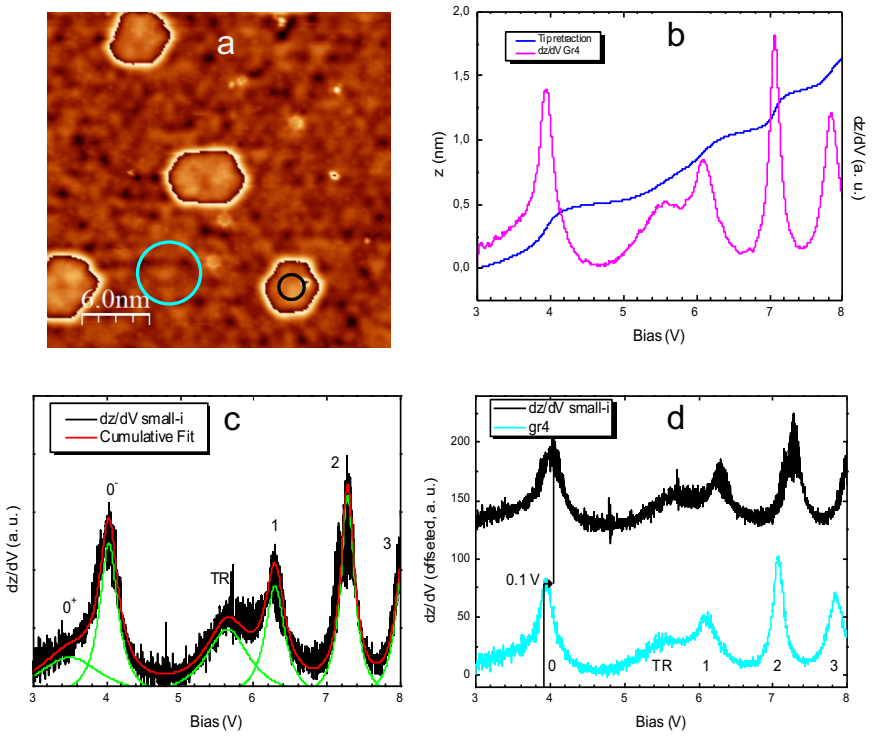

Figure 3: a) STM image of graphene and four small-islands (30x30 nm^2, 0.5 V, 0.4 nA). A flattening filter as been applied to amplify the corrugation. b) Average $z(V)$ and its numerical derivation dz/dV taken on gr4 area (circled blue in a). c) Determination of the IPS by adjusting (red) the experimental (black) dz/dV curves on the small-island circled in black in a) by six Lorentzian profiles (green), the IPSs numbering from 0 to 3 is perturbed by a transmission resonance (TR). d) Comparison of dz/dV spectra taken on small-islands and gr4.

3.2.2. Cobalt nanodots intercalated below graphene

In any case, the previous configuration is very different from the one formed by the cobalt atoms in the nanodots we present here. Depending on the initial amount of deposited Co, the annealing time and the temperature, size, height, shape and density of the nanodots can be varied. Here we will only detail their essential common characteristics, namely that they are encapsulated by graphene, which leads to important modifications in the electronic properties of graphene, as described in the following sections. A first nanodot, called nanodot1, is represented in Fig. A.5. A better resolution is obtained in Fig. 4a on a second nanodot, called nanodot2 in the following. Those nanodots exhibit two typical graphene fingerprints (those high-resolution STM images have been obtained in the measurements chamber). Firstly, some extended elongated defects (see upper right in Fig. A.5) are often seen after synthesis in UHV at high temperature [52]. Secondly, for nanodot2, we can see clearly in Fig. 5c two other identical defects very characteristic of graphene, the so-called "flower" defect. This defect is the smallest graphene boundary loop and can be seen as a $\pm\pi/6$ rotation of seven carbon

rings inside a regular MLG [39]. Those flowers appear generally on graphene after high-temperature annealing when foreign atoms are present, but can also be catalyzed in great quantity helped by metallic atoms, such as bismuth or gold [32].

An important point concerning these nanodots is the possibility that they are islands of oxidized cobalt, such as CoO, intercalated under a graphene plane. Indeed, the samples were exposed to air during their transfer between the two UHV chambers. Oxygen from the air could have interacted with the cobalt (mainly during the out-gassing of the samples after their introduction into the measurements chamber) by diffusing under the graphene surface and then chemically bonding to the Co islands (which, remember, were formed in the synthesis chamber). This possibility has already been studied by STM and XMCD [15]. Thus, it was shown that exposure of Co islands deposited on the graphene surface (SiC/BL/MLG/Co systems) to oxygen led to the formation of oxides, but that annealing at 650 °C was sufficient to deoxidize the cobalt and led to its intercalation in the form of small pure Co clusters (see also sec. 3.2.1). Here, our samples were obtained for slightly higher Co coverages than in this previous study, but our protocol is strictly identical. Thanks to AES measurements, an experimental confirmation of the absence of Oxygen after this protocol is exposed in Appendix D in the Supplementary file. We can therefore conclude that, although there was a passage through air, the degassing of the sample has removed oxygen.

Finally, we can note in Fig. 4a the proximity of BLG with nanodot2. This has been regularly observed near nanodots and recall intercalation experiments already performed for example on Co on the gr/Pt(111) or Ir(111)/oxide surface [28] or Mn on graphene on SiC(0001) [49]. These observations have been interpreted as the proto-formation of nanodots by isolated intercalated atoms between graphene and the substrate. This is obviously the previous small-islands which are the seeds of the nanodots. We can suppose that above a certain critical Co cluster size, the confined system of Co atoms and clusters will energetically prefer to form intercalated crystallites, the nanodots.

3.3. ***Spectroscopy of Image Potential States***

Here, we present tunnelling spectroscopy results obtained for bias voltages comprising between 1 and 8 V, *i.e.* the field emission regime. This allows us to deduce the local work function, W, by extracting the characteristic peaks of Image Potential States (IPS or FER, Field Effect Resonance) from measurements of the position z of the tip as a function of the bias voltage V. Classically, when electrons leave a conducting surface, the local redistribution of charges generates an attractive potential. If the energy of the electrons is lower than the work function, they cannot escape in the vacuum. However, in a quantum approach, energy levels are created by this potential. In a 1D charge image model, an image potential can be defined which IPS are hydrogenoid-like states and their energies relative to the Fermi level are given by Eq. 1).

$$E_n - E_F = W - \frac{0.85\ eV}{(n+a)^2} \tag{1}$$

with $W = E_{vac} - E_F$, a is a semi-empirical correction factor called "quantum defect" [46] and n a quantum number which indexes these IPS from $n = 0$ if $a \neq 0$. These states

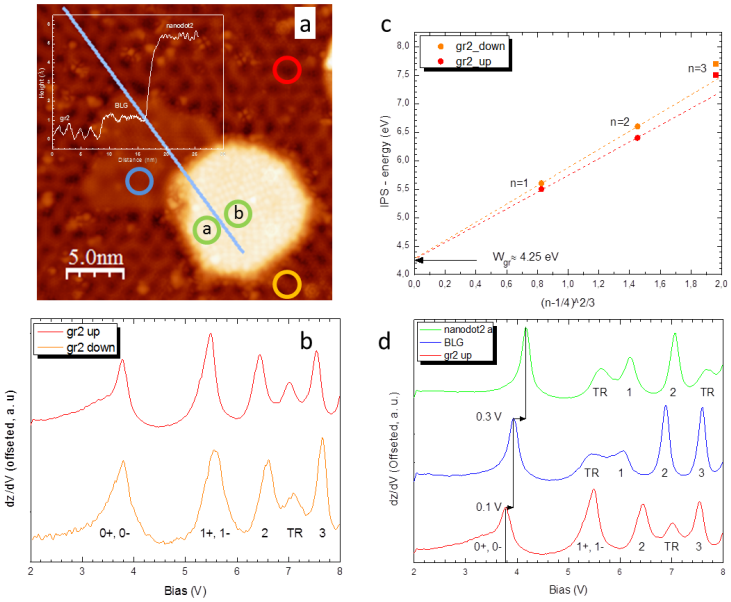

Figure 4: a) STM image of gr2 areas (orange and red), BLG (blue) and nanodot2 (green) (25x25 nm^2, 0.1 V, 300 pA) decorated with two "flower" defects (see details in Fig. 5), inset: height profile along the blue line. b) $dz/dV - V$ spectra from gr2-up and down in a. c) IPS energies relative to the Fermi Level on gr2-up and down (see also Tables T.1 and T.2 in Supplementary file Appendix B for all the IPS and Tunneling Resonance states (TR)), dotted lines are obtained using Eq. (2). Work functions for graphene areas are obtained from the common abscissa equal to 4.25 ± 0.1 eV. d) Shifts of 0.1 V and 0.3 V are indicated between the three respective first IPS numbered 0^- of gr2-up, BLG and nanodot2.

can be occupied (and studied) when electrons are added to or removed from the surface (for example by LEED, inverse photo-emission, two-photons photo-emission [84], field emission etc.). In this STS study, in order to have access to these states, we ramp the bias voltage between the tip and the sample keeping constant the tunnel current and we register simultaneously the tip retraction, $z(V)$. Because the current is related to the local tunnel current density (and to the shape of the tip [66], each time an IPS could be occupied, there is a step in the curve $z(V)$. However, the electric field induced between the tip and the sample generates an electrostatic potential that adds to the image potential and the previous virgin image potential is thus deformed. Consequently, it can be shown that the previous IPS are Starck shifted [33] but moreover, new states are created in the vacuum gap, the so-called Gundlach oscillations. An important point to notice is that the first IPS (observed at a low bias value, thus low z values) is generally hardly sensitive to the electric field because of the strong variation of the image potential with the distance perpendicular to the surface compared to the slower variation of the electrostatic potential induced by the STM tip. It follows that there are two ways to extract local work functions.

The first state (its associated wave function is localized very close to the geometric sample surface) is very sensitive to local work function variations induced by lo-

cal electronic environments of the surface (for example some underlying defects, surface/electronic corrugation such as moirés, interface states between the surface and the bulk). Therefore, we could compare its energy variation at various places on the surface in order to extract the corresponding work function variations relative to a starting value which serves as a reference, here it will be the one of a MLG. The second method is to use the semi-empirical formula, Eq. 2), which previous studies have shown to correctly describe higher-order FER peaks as follows [59, 56]:

$$eU_n = W + \left(\frac{3\pi he}{4\sqrt{2m}}\right)^{2/3} F^{2/3}(n - 1/4)^{2/3} \tag{2}$$

where F is the electric field of FER formation. Note that this formula is only valid for $n >> 1$ (thus at a large distance from the surface), but is generally used from $n = 1$ (this undoubtedly limits the model concerning absolute values of the work functions but not their relative values) because it conducts to a rather good approximation of the work function [65, 79, 56, 34].

In Figs. 3 and 4 we present measurements of $z(V)$ and its numerically derivative dz/dV obtained on different graphene areas, a small-island and a generic nanodot.

Fig. 3b shows the tip retraction, $z(V)$, as a function of the bias voltage (bias zero corresponds to the substrate Fermi level potential), measured on graphene4 area (gr4) circled in blue on Fig. 3a. Each vertical step can be accurately determined by the derivative function, dz/dV. Similar dz/dV taken on different graphene areas are reported in Fig. 3c. Following Borca et al. [34], we fitted these spectra with a series of Lorentzian profiles, see for example Fig. 3c obtained on the small-island circled in black on Fig. 3a.

We can immediately notice that the first peak numbered 0 (and in a less marked way numbered 1 in Figs. 4) is asymmetric and so must be fitted by two Lorentzian profiles (we obtain similar results with Gaussian or Voigt profiles), we label those features (0^+, 0^-) (and 1^+, 1^- in Fig. 4d) to remember that IPS theoretical calculations of freestanding monolayer graphene [76, 77] have proposed splitting of each IPS in couple indexed $n^\pm$ corresponding to the even or odd symmetry of those states relative to the geometric graphene plane. We choose this notation following the literature [35, 75].

In order to interpret more the other peaks, we turn to MLG regions displayed in Fig. 4a. This STM image involves MLG, BLG and a nanodot area, as well as a line profile across these three areas to indicate their apparent height differences. Fig. 4b shows two spectra acquired on the MLG area at two locations marked by the red (up) and orange (down) circles in Fig. 4a. Both spectra are similar and reveal four FER peaks and a Transmission Resonance (TR) signal around 7 V between FER peaks of second and third orders. Similar TR has also been observed for graphene on Rh(111) [85] and interpreted as a quantum-size effect in electron transmission through the adlayer constituted by a buried interface and the surface [61]. Note that usually, the intensity of TR is lower than that of FER making it easy to distinguish TR from FER.

However, whenever the TR appears, Eq. 2 is not valid for FER peaks with energies higher than the TR energy because the TR can shift them to higher energy, so-called TR-FER interplay [80]. Therefore, the third-order FER peak in Fig. 4b is excluded in the following work function analysis. Fig. 4c exhibits the energy versus $(n - 1/4)^{2/3}$

Area	MLG	BLG & Small i	Nanodots
Fingerprint	0 1 2 TR 3	0 TR 1 2 3	0 TR 1 2 TR
W (eV)	4.25 ± 0.1	4.35 ± 0.1	4.65 ± 0.1

plots for FER peaks of first and second orders in Fig. 4b. The slopes of two lines fitting the data points of two cases are not the same, indicating that the electric field F of the spectrum at the orange circle is stronger than that at the red circle. However, the extrapolated values of two fitting lines are nearly identical, reflecting that the value is insensitive to F, and thus, it can indicate that the work function of MLG is 4.25 ±0.10 eV.

Fig. 4d shows the spectra taken on BLG and nanodot areas at the locations marked by the blue and green circles, respectively, as well as the spectrum at the red circle on MLG area for comparison. There are some differences between them. In the spectrum of BLG, the TR signal is changed to appear between FER peaks of zeroth and first orders, which is the same for the spectrum of nanodot. However, there is an additional TR signal appearing above the energy of FER peak of second order in the spectrum of nanodot, which may originate from the graphene/Co interface property. Because of the TR-FER interplay, the energies of FER peaks of first and second orders cannot be used to extract the work functions of BLG and nanodot through Eq. 2.

A previous study proved that the energy shift between zero-order FER peaks is not precisely equal to the work function difference of a heteroepitaxial metal on a metallic substrate, but that those of higher orders are [65]. Moreover, a recent study on a hBN monolayer with moiré patterns revealed that the zero-order energy shift can be equal to that of higher orders for different locations on the moiré pattern [89]. This result can be interpreted as the fact that *for the same material*, the zero-order energy shift can represent the difference in work function. Similarly, in our case, MLG, BLG, and graphene on Co can also be considered as a single carbon plane in contact with different interfaces. Therefore, the energy shifts of the zeroth-order FER peaks can indicate their work function differences. Fig. 4d shows that the energy shift of zeroth order is 0.1 ± 0.1 eV for MLG and BLG, and the one is 0.3 ± 0.1 eV for BLG and nanodot. Because the work function of MLG is 4.25 ± 0.1 eV, those of BLG and nanodot are 4.35 ± 0.1 and 4.65 ± 0.1 eV, respectively. Moreover, in comparison to the spectrum of BLG, it can be known that the gr4 area in Fig. 3a is BLG. Therefore, the work function of small-i is determined to be 4.35 ± 0.1 eV through the energy shift of zeroth order in Fig. 3d. All those results are summarized in the following table (see all indexed IPS and TR energy positions in Tables T.1 and T.2 in Supplementary file Appendix B.).

The first point to observe is that our STM/STS measurement of $W_{gr} \simeq 4.25 \pm 0.1$ eV is compatible with previous ARPES measurements, *i.e*. 4.28 and 4.16 eV [40, 69] and slightly above the value of 4.05 eV measured by 2PPE [51]. Moreover, the calculated freestanding graphene work function has been calculated to be 4.5 eV [58]. If we suppose a rigid shift of the graphene band structure induced by the n-doping of the underlying BL/SiC substrate, we could expect a decrease in the MLG work function as effectively observed here. Concerning the BLG, Kelvin probe force microscopy [47] has shown a difference of 0.15 eV between the MLG and BLG work functions. Our results are also consistent with this shift which has been interpreted as a screening of

the substrate. We can expect that by increasing the number of graphene layers, W evolves towards that of graphite, 4.6 eV, a commonly accepted value [57]. In Fig. C.5, our DFT calculations show indeed a similar trend.

The second point concerns nanodots. The increase of the work function (from 4.25 ± 0.1 to 4.65 ± 0.1 eV) induced by intercalated Co could be expected since the bulk Co work function, 5.5 eV [82], is greater than that of graphene and so electrons of the graphene being attracted by the underlying Co are more difficult to extract toward the vacuum level leading to an increase in the work function. However, this value is greater than the calculated value of 4.5 eV. It means that the graphene becomes slightly p-doped. Moreover, as we will see later, the Co intercalation has conducted to nearly neutralize the graphene over-layer. This Co p-doping contribution balancing the SiC n-doping and increasing the work function has already been observed for tetrafluoro-tetracyanoquin-odimethane (F4-TCNQ) adsorption on graphene on SiC and can be explained by a charge transfer from graphene to the molecular layer [37]. Our result is rather unexpected compared to theoretical calculations of the electronic properties of graphene on Co(0001) which predict that a graphene layer on this surface has a work function of 3.8 eV. [50]. But, it is also predicted that Co(0001)-Gr interactions are so strong due to hybridization between their orbitals which results in the disappearance of the Dirac cone [58]. Similar destructions of the electronic properties of graphene on Fe/Ir(111) [45] or Ni [31] have also been observed, but we will show in 3.4 that since we are not in these cases of metallic substrates, our situation is completely different. Thanks to DFT calculations presented later, we will prove that in fact, nanodots can be interpreted as two Co atomic planes intercalated between a quasi-decoupled carbon plane and the BL.

3.4. ***Spectroscopy and DOS near the Fermi level***

In this section, we present results from STS. In particular, we discuss how the dI/dV spectra evolve from MLG to BLG and nanodots and how they can be compared to the DOS calculated by DFT, especially for BLG, where we will show that all our measurements can be interpreted as two cobalt layers intercalated below a quasi-freestanding MLG and partially coupled to the BL, leaving the SiC substrate being unaltered. Fig. 5a displays representative dI/dV curves of various circled areas measured in Fig. 4a.

The spectra shown in that figure are averages of spectra taken over several points, and the corresponding STM images of these three areas are displayed in Figs. 5c, d and e. We first notice that all spectra present a minimum at zero bias but exhibit two different shapes. On MLG and BLG, a clear phonon pseudo-gap (with a width around 130 meV due to the inelastic excitation of an acoustic phonon of graphene) is clearly defined contrary to the V-shaped behavior measured on the nanodot (note that all explored nanodots display this same spectrum). Despite the fact that nanodots are covered by graphene, the pseudo-gap is not apparent. This V-shape is obviously a clear signature of the graphene charge neutrality point and the absence of the phonon-gap for decoupled graphene from its substrate has been predicted theoretically [86]. On the MLG area, a second minimum is measured around -0.5 eV. This minimum is attributed to the graphene Dirac point, as already observed in the past for this n-doped graphene [36]. This minimum is shifted to lower energy for the BLG [62, 74] and finally to zero

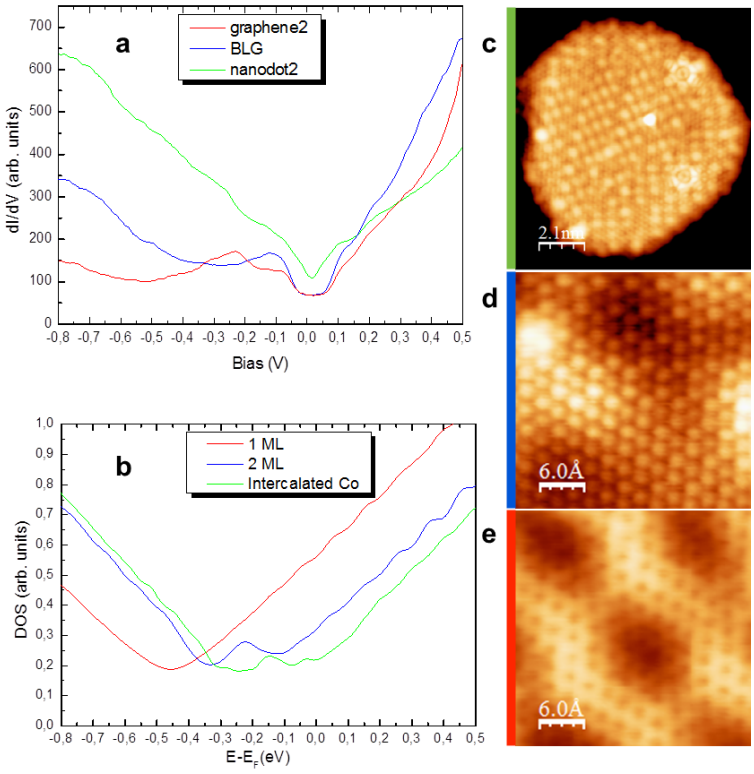

Figure 5: a) dI/dV spectra recorded at the same spots as in Fig. 4a on nanodot2 (green), BLG (blue) and gr2-up area (red). The energy minima on graphene2 and BLG in the occupied states are indications of the Dirac points. On the nanodot, a clear V-shaped curve is centered at the Fermi level. Zooms of Fig. 4a corresponding to these curves are respectively reported in c (10x12 nm^2), d (3x3 nm^2) and e (3x3 nm^2). All STM images were recorded at 0.1 V, 300 pA. b) Calculated DOS for MLG and BLG over a buffer layer on SiC(0001) (see also Figures C.1 to C.5) and the calculated DOS of the configuration SiC/BL/bilayer Co/BLG reported in Fig. 6 and framed in red.

for the nanodot. Note that there is no peak around the Fermi level for both graphene spectra as could be observed for an oxidized sample. Indeed, this type of peak could be the signature of oxygen incorporation in the SiC substrate [29]. As there is no peak, we can assume that our samples have not been in a condition to be oxidized (simultaneously exposed to O_2 and high temperature) as already mentioned in Sec.3.2.2. As far as nanodots are concerned, we cannot have access to the atomic positions of Co and therefore we performed DFT calculations on different configurations presented here and in Supplementary file Appendix C.

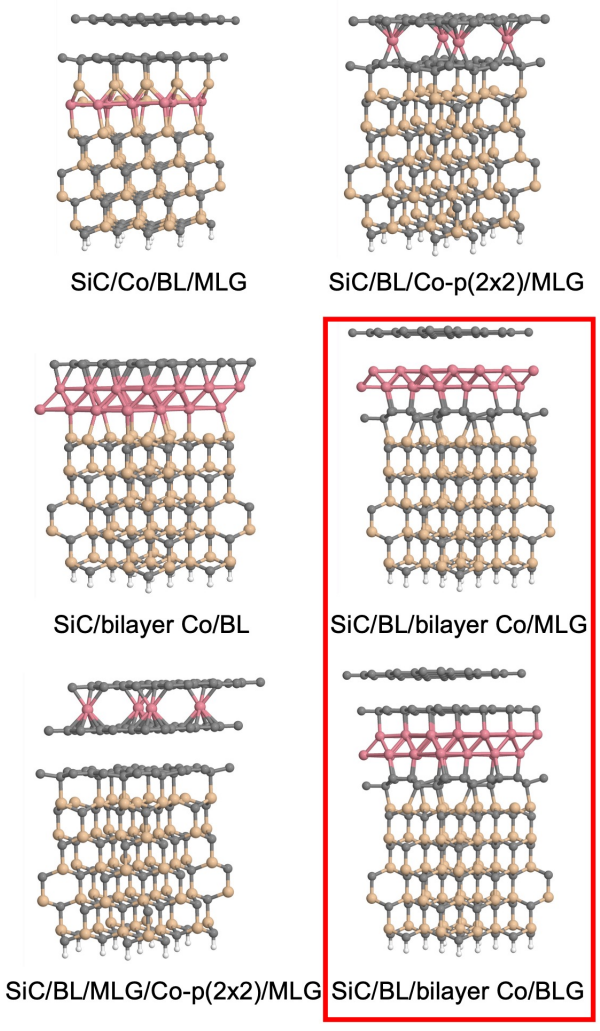

Figure 6: Relaxed atomic configurations from DFT calculations of various Co intercalated models. The calculated corresponding DOS are reported in Fig. C.6. The configurations that correspond to all our experimental measurements are framed in red.

Firstly, we calculated DOS(n) of SiC/BL/n-MLG which is a stacking of n (ranging from 1 to 10) graphene layers (forming an hcp structure) on the buffer-layer over SiC (see supplementary file Figs. C.1 to C.5). To this end we have considered a 3x3 unit cell of 5 layers SiC, on top of which we have set a buffer layer which presents one-third of its carbon atoms bonded to the underneath silicon atoms. Considering the buffer layer in A position, we have set a graphene layer in B position, and all the next graphene layers for the different calculations have been set following an ABABAB... stacking. Finally, a set of 300 specific k-points along the Γ-K-M path has been used for band structure calculations. For the first graphene monolayer, the Dirac point has been determined using the position of the Dirac cone. However, for 2 mono-layers and more, a gap is opened in the total band structure due to the charge symmetry breaking between the different graphene layers (see also Supplementary file Appendix C). Therefore, the Dirac point for these configurations has been determined from the Partial Density of States calculation of the top graphene layer. As expected, the Dirac point, which is marked in the DOS by a minimum around -0.45 eV relative to the Fermi position for $n = 1$, shifts towards lower energy when n increases (see Supplementary file Fig. C.5). The calculated work function for SiC/BL/BLG is 0.06 eV higher than the work function for the SiC/BL/MLG configuration. This shift is comparable to the experimental shift of 0.1 eV between MLG and BLG. Note that in the following we used the experimental value of 4.25 ± 0.1 eV for MLG as a reference for the calculated W values.

Then, we calculated DOS, work functions and explored the stability of the following configurations:
SiC/Co/BL/MLG : Co substituted to C atoms in the first SiC layer, MLG on AB stacking with ZLG;
SiC/BL/Co-p(2x2)/MLG : Co atoms in hollow sites between the BL and MLG;
SiC/bilayer Co/MLG : Co AB bilayer on top of SiC, MLG on top;
SiC/BL/bilayer Co/MLG : Co AB bilayer on top of BL, MLG on top;
SiC/BL/MLG/Co-p(2x2)/MLG : ABAB stacking of 2 MLG on SiC/BL with Co intercalated in the hollow sites of the two MLGs;
SiC/BL/bilayer Co/BLG : ABAB stacking of 2 MLG on SiC/BL with Co AB bilayer intercalated on top of the BL.

All those configurations are stable (*i.e.* convergence of the relaxed structures) contrary to the following configurations which are found to be unstable: SiC/Co/BL, SiC/BL/Co-p(1x1)/BLG and SiC/BL/MLG/Co-p(1x1)/MLG (not represented). The former could be in fact an intermediate unstable situation towards CoSi alloying [18] as reported in the SiC/Co/BL/MLG configuration (cf. Fig.6).

The latter has been proposed in the past but was not optimized [16]. Fig. 6 shows side views of these Co intercalated models once fully relaxed. In order to discriminate between these configurations, we selected two criteria: i) a DOS as close as possible to our results on nanodots as reported in Fig. 5a and, ii) a calculated W very close to the experimental value deduced from the IPS of the nanodots. Thus, among those configurations (see all calculated DOS in the Supplementary file Appendix C, Fig. C.6), there are only the SiC/BL/bilayer Co/MLG ($W = 4.47$ eV) and SiC/BL/bilayer Co/BLG ($W = 4.76$ eV) which satisfied those criteria. In Fig. 5b we reported the calculated DOS for SiC/BL/MLG, SiC/BL/BLG and SiC/BL/bilayer Co/BLG. The comparison

with our experimental results is quite correct. In order to separate these two remaining possibilities, we can remark that a careful examination of the nanodot image in Fig. 5c reveals the presence of small areas free of moiré (for example at the bottom) where the characteristic Bernal (AB) stacking of BLG is clearly visible. Finally, except for this point, our experimental measurements and DFT results did not allow us to discriminate precisely between these two situations (this point is also discussed below concerning the nanodot heights). But, in any case, we can conclude that all these observations (STM topography), measurements (dz/dV and dI/dV) and DFT calculations converge towards this exceptional and unexpected intercalation of a bilayer Co between carbon planes, the upper one being almost decoupled from the underlying planes.

Finally, thanks to our DFT calculations, we can interpret the apparent height of nanodots relative to the surrounding MLG area. For the stacking SiC/BL/bilayer Co/MLG, the calculated inter-plane distances are: BL-Co = 2.20 ± 0.05 Å; Co-Co = 1.40 ± 0.05 Å; Co-MLG = 3.35 ± 0.05 Å. For the stacking SiC/BL/bilayer Co/BLG, we find: BL-Co = 2.20 ± 0.05 Å; Co-Co = 1.64 ± 0.05 Å; Co-BLG = 2.20 ± 0.05 Å. Thus, the total distances between the BL and the top of these two stackings are resp. around 6.95 and 9.45 Å. Taking into account the inter-plane distance of 3.4 Å between the BL and an MLG layer, the calculated heights relative to an MLG (with the same SiC plane as a reference, see the sketches in Fig. A.5c and f in the Supplementary file) are around 3.6 and 6.1 Å, respectively. The heights of our experimental values for nanodots 1 and 2 are resp. 3.5 and 5.5 Å. The comparison is quite correct. Two points should be noted. First, we explored only a few nanodots and their heights relative to the surrounding areas varied between 3.5 and 9 Å. Second, it is very possible that some nanodots reside on a SiC terrace that is 2.5 Å higher or lower than the surrounding SiC terrace. This leads to the conclusion that there is indeterminacy about the exact number of graphene planes on top of a Co bilayer (see Fig. A.5f in the supplementary file, which shows two possible stacks that nevertheless lead to the same result).

3.5. ***Discussion about the apparent moirés on nanodots***

The last point to discuss regarding the nanodots encapsulated in graphene is their peculiar moiré-like atomic texture (see Fig. 5c). Graphene moirés have been frequently observed on the carbon-rich SiC$(000\bar{1})$ face [54] or by transfer, within a top-down approach, from one MLG to another MLG with very precise control of the azimuthal angle between both. Moirés of graphene on metallic substrates have been studied extensively [87], but to our knowledge, they were never observed so far on a Co surface (because of a too-small misfit of 2% and strong coupling between Co and graphene) nor on Co intercalated graphene on metallic surfaces, certainly because the intercalated Co are in perfect registry with the substrate, for example on ruthenium [64]. However, striped moiré such as on nanodot1 (see Supplementary file Fig. A.5) and hexagonal moiré have been observed respectively on graphene on Ni(110) and Ni(111) faceted islands of few nm heights on graphite [71]. Here, as seen more precisely in Fig. 5c, "moirés" present a rectangular symmetry, which is rather unexpected for graphene on dense cobalt atomic planes. The interpretation of this moiré is not the central part of this article and deserves in-depth analysis, but we can propose two possible interpretations.

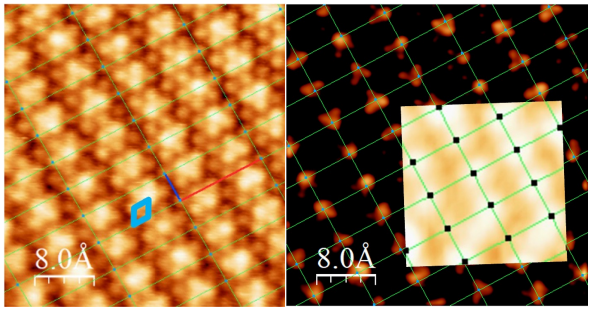

(a) (b)

Figure 7: (a) Atomic resolution on nanodot3 (4x4 nm^2, 0.05 V, 800 pA). Blue rhombus depicts a graphene unit cell, blue (4.7 ± 0.1Å) and red (12.8 ± 0.1Å) perpendicular vectors depict the unit cell of the superstructure (see also Appendix A, Fig. A.6 in the Supplementary file). (b) Same as 7a but thresholded to emphasize that the apparent moiré of nanodot2, plotted in the inset, is actually the position of the highest local electron density.

It is important to note that the moirés of nanodots 1 and 2 are only apparent moirés. Thus, in Fig. 7a taken on another nanodot (nanodot3) at a very low tunnelling voltage, 50 mV, the atomic texture is revealed, and we find locally a hexagonal pattern but modulated in a periodic way. The modulation is complex and systematic voltage analysis as well as STM image calculations by DFT are in progress (see below). It should be noted, however, that a simple thresholding effect on the topography, cf. Fig. 7b, leads to obtain a texture identical to that of the nanodot2 of Fig. 5c (obtained at 1 V) and superimposed in the insert, namely a breaking of the hexagonal symmetry (hc) observed locally (Fig. 7a) and the appearance of an orthorhombic lattice (op) (Fig. 7b). Note that this rectangular texture is also observed on other nanodots synthesized in the synthesis chamber (see Fig. A.6 of the Supplementary file), thus before transfer to the measurement chamber. If it were necessary, this is an additional argument to reject the hypothesis of oxidation of intercalated cobalt nanodots during the transfer between the two chambers. This symmetry breaking can have several origins: i) crystallographic, ii) chemical or iii) electronic. Case i) has been explored in Sec. 3.4 (see also Supplementary file Fig. C.6), although not exhaustively given a large number of possible configurations, by eliminating unstable structures with respect to relaxation calculations. The conclusion on the compact bilayer of Co atoms between two carbon planes, however, seems to us to explain all our measurements described above, although additional more detailed calculations based on a hypothesis of correlated electrons could be envisaged to try to reproduce the atomic or electronic modulation observed. The possibility of a moiré induced by the superposition of a graphene plane with a sub-layer of Oxide (CoO), Carbide (CoC), or Silicide (CoSi) composition, case ii), is possible. This point could be definitively settled by complementary XPS measurements. For oxides, AES measurements reported in Appendix D of the supplementary file, within the limited sensitivity of this technique, excluded oxygen contamination. Moreover, according to the literature, each of these three cases seems unlikely. For CoO the structure is hexagonal [44], this symmetry should thus appear in all the images, which is

not the case. If we compare with the graphene/oxygen/Ni(111) system observed by STM [60], there is certainly the formation of an oxide (obtained by oxygen exposure and by annealing between 120 and 250 , which is not the case here) but, again, the hexagonal symmetry is preserved. For the two other chemical alternatives, the carbon or silicon atoms can only come from the underlying SiC during annealing. However, the annealing has always been carried out between 900-950°C at temperatures below that of the decomposition of SiC, around 1150 °C [81, 70]. We can therefore exclude the chemical origin of the modulation.

There remains case iii) of a purely electronic phenomenon linked to the formation of the sandwich carbon plane - bilayer Co - carbon plane. It is well known that for Bernal stacked graphite, practically only 1 atom out of 2 is visible by STM, especially at low voltage, because of the coupling with the carbon plane atoms under the surface plane. Just as the p(6x6) structure of the ZLG visible by STM is not a moiré but of purely electronic origin, we can assume that the atomic structure retained by our calculations (cf. Fig. 6 the red layout), namely a sandwich carbon plane - bilayer Co - carbon plane, must also lead to a modulation of the electronic coupling according to the underlying stacking. In other words, the LDOS should be spatially modulated. A preliminary calculation of STM images is shown in Appendix C, Figure C.7 of the Supplementary file for the SiC/BL/bilayer Co/MLG configuration. Despite the small p(3x3) unit cell used to calculate the DOS (see Methods), a rectangular symmetry is evidenced. Only tunnelling calculations on larger unit cells could then explain the modulations observed on the nanodots. Finally, we note the remarkable similarity between Fig. 7a and STM measurements performed on systems showing charge density waves, for example, a VS2 monolayer on graphene on Ir(111) [83] or CaC6 surface [73]. This similarity is not proof, but we believe that only purely electronic interactions are at the origin of the observed periodic modulation, while preserving the characteristics of graphene (i.e. no hybridization). [28]

Conclusion

The intercalation of cobalt between graphene and the buffer layer on SiC(0001) conducts to two different situations depending on the local Co atom concentration: intercalated clusters of a few atoms forming small-islands, and nanodots. The STM imaging shows, on one hand, that the clusters have a very narrow size dispersion and atomic height and, on the other hand, that the nanodots have a size of a few nm and heights compatible with two cobalt planes covered by one or two carbon planes. These nanodots show apparent moiré patterns whose rectangular symmetry is not yet fully understood, which deserves further study. Spectroscopic measurements of local conductance and work function show that graphene is n-doped without cobalt and that it loses its doping progressively for intercalation of isolated atoms to a quasi-neutrality for the nanodots, cobalt acting as a p-dopant. Correlatively, the work function increases from 4.25 eV for a monolayer of graphene without cobalt to 4.65 eV on the nanodots. DFT calculations of the electronic band structures and density of states of graphene multilayers on SiC with and without intercalated Co atoms confirm that the nanodots are intercalated bilayer Co islands between a quasi-freestanding graphene and the buffer

layer. The electronic graphene structure is preserved and the Dirac point energy is zero leaving a neutral graphene.

Acknowledgments

We are grateful to the ANR and MOST (DEFINE2D Project No. ANR-20-CE09-0023, MOST No. 110-2923-M- 002 -010) for financial support.

Appendix: Supplementary data

The following are the Supplementary data to this article:

Supplementary file presents three Appendices:

Appendix A reports STM characterization of graphene on a buffer layer and intercalated nanodots.

Appendix B reports the tables of Image Potential Surface states.

Appendix C reports results of Density Functional Theory calculations.

Appendix D reports Auger electron spectroscopy of cobalt and oxygen at different stages of sample preparation.

All these Appendixes can be downloaded.

References

[1] D. M. Kennes, M. Claassen, L. Xian, A. Georges, A. J. Millis, J. Hone, C. R. Dean, D. N. Basov, A. N. Pasupathy, A. Rubio, Moiré heterostructures as a condensed-matter quantum simulator, Nature Physics 17 (2) (2021) 155–163. doi:10.1038/s41567-020-01154-3.

[2] T. S. Sreeprasad, V. Berry, How Do the Electrical Properties of Graphene Change with its Functionalization?, Small 9 (3) (2013) 341–350. doi:10.1002/smll.201202196.

[3] H. Yang, G. Chen, A. A. C. Cotta, A. T. N'Diaye, S. A. Nikolaev, E. A. Soares, W. A. A. Macedo, K. Liu, A. K. Schmid, A. Fert, M. Chshiev, Significant Dzyaloshinskii–Moriya interaction at graphene–ferromagnet interfaces due to the Rashba effect, Nature Materials 17 (7) (2018) 605–609. doi:10.1038/s41563-018-0079-4.

[4] D. Khokhriakov, A. M. Hoque, B. Karpiak, S. P. Dash, Gate-tunable spin-galvanic effect in graphene-topological insulator van der Waals heterostructures at room temperature, Nature Communications 11 (1) (2020) 3657. doi:10.1038/s41467-020-17481-1.

[5] J.-F. Dayen, S. J. Ray, O. Karis, I. J. Vera-Marun, M. V. Kamalakar, Two-dimensional van der Waals spinterfaces and magnetic-interfaces, Applied Physics Reviews 7 (1) (2020) 011303. doi:10.1063/1.5112171.

[6] H. Kim, O. Dugerjav, A. Lkhagvasuren, J. M. Seo, Charge neutrality of quasi-free-standing monolayer graphene induced by the intercalated Sn layer, Journal of Physics D: Applied Physics 49 (13) (2016) 135307. doi:10.1088/0022-3727/49/13/135307.

[7] P. Gallagher, C.-S. Yang, T. Lyu, F. Tian, R. Kou, H. Zhang, K. Watanabe, T. Taniguchi, F. Wang, Quantum-critical conductivity of the Dirac fluid in graphene, Science 364 (6436) (2019) 158–162. doi:10.1126/science.aat8687.

[8] P. U. Asshoff, J. L. Sambricio, A. P. Rooney, S. Slizovskiy, A. Mishchenko, A. M. Rakowski, E. W. Hill, A. K. Geim, S. J. Haigh, V. I. Fal'ko, I. J. Vera-Marun, I. V. Grigorieva, Magnetoresistance of Vertical Co-graphene-NiFe Junctions Controlled by Charge Transfer and Proximity-Induced Spin Splitting in Graphene, 2D Materials 4 (3) (2017) 031004. doi:10.1088/2053-1583/aa7452.

[9] D. Eom, D. Prezzi, K. T. Rim, H. Zhou, M. Lefenfeld, S. Xiao, C. Nuckolls, M. S. Hybertsen, T. F. Heinz, G. W. Flynn, Structure and Electronic Properties of Graphene Nanoislands on Co(0001), Nano Letters 9 (8) (2009) 2844–2848. doi:10.1021/nl900927f.

[10] D. Prezzi, D. Eom, K. T. Rim, H. Zhou, M. Lefenfeld, S. Xiao, C. Nuckolls, T. F. Heinz, G. W. Flynn, M. S. Hybertsen, Edge Structures for Nanoscale Graphene Islands on Co(0001) Surfaces, ACS Nano 8 (6) (2014) 5765–5773. doi:10.1021/nn500583a.

[11] W. Chen, K. P. Loh, H. Xu, A. T. S. Wee, Growth of monodispersed cobalt nanoparticles on 6H–SiC(0001) honeycomb template, Applied Physics Letters 84 (2) (2004) 281–283. doi:10.1063/1.1639508.

[12] S. W. Poon, W. Chen, E. S. Tok, A. T. S. Wee, Probing epitaxial growth of graphene on silicon carbide by metal decoration, Applied Physics Letters 92 (10) (2008) 104102. doi:10.1063/1.2883941.

[13] S. W. Poon, A. T. Wee, E. S. Tok, Anomalous scaling behaviour of cobalt cluster size distributions on graphite, epitaxial graphene and carbon-rich $(6\sqrt{3}\times6\sqrt{3})$R30°, Surface Science 606 (21-22) (2012) 1586–1593. doi:10.1016/j.susc.2012.06.011.

[14] T. Eelbo, M. Waśniowska, M. Gyamfi, S. Forti, U. Starke, R. Wiesendanger, Influence of the degree of decoupling of graphene on the properties of transition metal adatoms, Physical Review B 87 (20) (2013) 205443. doi:10.1103/PhysRevB.87.205443.

[15] L. H. de Lima, R. Landers, A. de Siervo, Patterning Quasi-Periodic Co 2D-Clusters underneath Graphene on SiC(0001), Chemistry of Materials 26 (14) (2014) 4172–4177. doi:10.1021/cm501976b.

[16] Y. Zhang, H. Zhang, Y. Cai, J. Song, P. He, The investigation of cobalt intercalation underneath epitaxial graphene on 6H-SiC(0 0 0 1), Nanotechnology 28 (7) (2017) 075701. doi:10.1088/1361-6528/aa53c3.

[17] R. Hönig, P. Roese, K. Shamout, T. Ohkochi, U. Berges, C. Westphal, Structural, chemical, and magnetic properties of cobalt intercalated graphene on silicon carbide, Nanotechnology 30 (2) (2019) 025702. doi:10.1088/1361-6528/aae8c9.

[18] A. A. Rybkina, S. O. Filnov, A. V. Tarasov, D. V. Danilov, M. V. Likholetova, V. Yu. Voroshnin, D. A. Pudikov, D. A. Glazkova, A. V. Eryzhenkov, I. A. Eliseyev, V. Yu. Davydov, A. M. Shikin, A. G. Rybkin, Quasi-freestanding graphene on SiC(0001) via cobalt intercalation of zero-layer graphene, Physical Review B 104 (15) (2021) 155423. doi:10.1103/PhysRevB.104.155423.

[19] N. Briggs, Z. M. Gebeyehu, A. Vera, T. Zhao, K. Wang, A. De La Fuente Duran, B. Bersch, T. Bowen, K. L. Knappenberger, J. A. Robinson, Epitaxial graphene/silicon carbide intercalation: a minireview on graphene modulation and unique 2D materials, Nanoscale 11 (33) (2019) 15440–15447. doi:10.1039/C9NR03721G.

[20] L. Daukiya, M. N. Nair, M. Cranney, F. Vonau, S. Hajjar-Garreau, D. Aubel, L. Simon, Functionalization of 2D materials by intercalation, Progress in Surface Science 94 (1) (2019) 1–20. doi:10.1016/j.progsurf.2018.07.001.

[21] C. Berger, W. A. de Heer, Flat and safe under the graphene sheet, Nature Materials 19 (6) (2020) 583–584. doi:10.1038/s41563-020-0666-z.

[22] S. Forti, S. Link, A. Stöhr, Y. Niu, A. A. Zakharov, C. Coletti, U. Starke, Semiconductor to metal transition in two-dimensional gold and its van der Waals heterostack with graphene, Nature Communications 11 (1) (2020) 2236. doi:10.1038/s41467-020-15683-1.

[23] S. Ichinokura, K. Sugawara, A. Takayama, T. Takahashi, S. Hasegawa, Superconducting Calcium-Intercalated Bilayer Graphene, ACS Nano 10 (2) (2016) 2761–2765. doi:10.1021/acsnano.5b07848.

[24] J. C. Kotsakidis, A. Grubišić-Čabo, Y. Yin, A. Tadich, R. L. Myers-Ward, M. DeJarld, S. P. Pavunny, M. Currie, K. M. Daniels, C. Liu, M. T. Edmonds, N. V. Medhekar, D. K. Gaskill, A. L. Vázquez de Parga, M. S. Fuhrer, Freestanding n-Doped Graphene via Intercalation of Calcium and Magnesium into the Buffer Layer–SiC(0001) Interface, Chemistry of Materials 32 (15) (2020) 6464–6482. doi:10.1021/acs.chemmater.0c01729.

[25] G. S. Grebenyuk, E. Yu. Lobanova, D. A. Smirnov, I. A. Eliseev, A. V. Zubov, A. N. Smirnov, S. P. Lebedev, V. Yu. Davydov, A. A. Lebedev, I. I. Pronin, Cobalt Intercalation of Graphene on Silicon Carbide, Physics of the Solid State 61 (7) (2019) 1316–1326. doi:10.1134/S1063783419070102.

[26] G. Sclauzero, A. Pasquarello, Carbon rehybridization at the graphene/SiC(0001) interface: Effect on stability and atomic-scale corrugation, Physical Review B 85 (16) (2012) 161405. doi:10.1103/PhysRevB.85.161405.

[27] L. H. de Lima, A. de Siervo, R. Landers, G. A. Viana, A. M. B. Goncalves, R. G. Lacerda, P. Häberle, Atomic surface structure of graphene and its buffer layer on SiC(0001): A chemical-specific photoelectron diffraction approach, Physical Review B 87 (8) (2013) 081403. doi:10.1103/PhysRevB.87.081403.

[28] F. Ajejas, A. Anadon, A. Gudin, J. M. Diez, C. G. Ayani, P. Olleros-Rodríguez, L. de Melo Costa, C. Navío, A. Gutierrez, F. Calleja, A. L. Vázquez de Parga, R. Miranda, J. Camarero, P. Perna, Thermally Activated Processes for Ferromagnet Intercalation in Graphene-Heavy Metal Interfaces, ACS Applied Materials & Interfaces 12 (3) (2020) 4088–4096. doi:10.1021/acsami.9b19159.

[29] I. Antoniazzi, T. Chagas, M. J. S. Matos, L. A. B. Marçal, E. A. Soares, M. S. C. Mazzoni, R. H. Miwa, J. M. J. Lopes, Â. Malachias, R. Magalhães-Paniago, M. H. Oliveira, Oxygen intercalated graphene on SiC(0001): Multiphase SiOx layer formation and its influence on graphene electronic properties, Carbon 167 (2020) 746–759. doi:10.1016/j.carbon.2020.05.064.

[30] M. Basanta, Y. Dappe, P. Jelínek, J. Ortega, Optimized atomic-like orbitals for first-principles tight-binding molecular dynamics, Computational Materials Science 39 (4) (2007-06, 2007) 759–766. doi:10.1016/j.commatsci.2006.09.003.

[31] M. Batzill, The surface science of graphene: Metal interfaces, CVD synthesis, nanoribbons, chemical modifications, and defects, Surface Science Reports 67 (3) (2012) 83–115. doi:10.1016/j.surfrep.2011.12.001.

[32] Q. Berrahal, C. Chacon, H. Amara, A. Bellec, S. Latil, V. Repain, S. Rousset, J. Lagoute, Y. Girard, High density synthesis of topological point defects in graphene on 6H–SiC(0001^{-}), Carbon 170 (2020) 174–181. doi:10.1016/j.carbon.2020.08.008.

[33] G. Binnig, K. H. Frank, H. Fuchs, N. Garcia, B. Reihl, H. Rohrer, F. Salvan, A. R. Williams, Tunneling Spectroscopy and Inverse Photoemission: Image and Field States, Physical Review Letters 55 (9) (1985) 991–994. doi:10.1103/PhysRevLett.55.991.

[34] B. Borca, C. Castenmiller, M. Tsvetanova, K. Sotthewes, A. N. Rudenko, H. J. W. Zandvliet, Image potential states of germanene, 2D Materials 7 (3) (2020) 035021. doi:10.1088/2053-1583/ab96cf.

[35] S. Bose, V. M. Silkin, R. Ohmann, I. Brihuega, L. Vitali, C. H. Michaelis, P. Mallet, J. Y. Veuillen, M. A. Schneider, E. V. Chulkov, P. M. Echenique, K. Kern, Image potential states as a quantum probe of graphene interfaces, New Journal of Physics 12 (2) (2010) 023028. doi:10.1088/1367-2630/12/2/023028.

[36] V. W. Brar, Y. Zhang, Y. Yayon, T. Ohta, J. L. McChesney, A. Bostwick, E. Rotenberg, K. Horn, M. F. Crommie, Scanning tunneling spectroscopy of inhomogeneous electronic structure in monolayer and bilayer graphene on SiC, Applied Physics Letters 91 (12) (2007) 122102. doi:10.1063/1.2771084.

[37] W. Chen, S. Chen, D. C. Qi, X. Y. Gao, A. T. S. Wee, Surface Transfer p-Type Doping of Epitaxial Graphene, Journal of the American Chemical Society 129 (34) (2007) 10418–10422. doi:10.1021/ja071658g.

[38] W. Chen, H. Xu, L. Liu, X. Gao, D. Qi, G. Peng, S. C. Tan, Y. Feng, K. P. Loh, A. T. S. Wee, Atomic structure of the 6H–SiC(0001) nanomesh, Surface Science 596 (1-3) (2005) 176–186. doi:10.1016/j.susc.2005.09.013.

[39] E. Cockayne, G. M. Rutter, N. P. Guisinger, J. N. Crain, P. N. First, J. A. Stroscio, Grain boundary loops in graphene, Physical Review B 83 (19) (2011) 195425. doi:10.1103/PhysRevB.83.195425.

[40] C. Coletti, C. Riedl, D. S. Lee, B. Krauss, L. Patthey, K. von Klitzing, J. H. Smet, U. Starke, Charge neutrality and band-gap tuning of epitaxial graphene on SiC by molecular doping, Physical Review B 81 (23) (2010) 235401. doi:10.1103/PhysRevB.81.235401.

[41] Y. J. Dappe, Y. Almadori, M. T. Dau, C. Vergnaud, M. Jamet, C. Paillet, T. Journot, B. Hyot, P. Pochet, B. Grévin, Charge transfers and charged defects in WSe_2/graphene-SiC interfaces, Nanotechnology 31 (25) (2020) 255709. doi:10.1088/1361-6528/ab8083.

[42] Y. J. Dappe, J. Ortega, F. Flores, Intermolecular interaction in density functional theory: Application to carbon nanotubes and fullerenes, Physical Review B 79 (16) (2009) 165409. doi:10.1103/PhysRevB.79.165409.

[43] M. T. Dau, M. Gay, D. Di Felice, C. Vergnaud, A. Marty, C. Beigné, G. Renaud, O. Renault, P. Mallet, T. Le Quang, J.-Y. Veuillen, L. Huder, V. T. Renard, C. Chapelier, G. Zamborlini, M. Jugovac, V. Feyer, Y. J. Dappe, P. Pochet, M. Jamet, Beyond van der Waals Interaction: The Case of $MoSe_2$ Epitaxially Grown on Few-Layer Graphene, ACS Nano 12 (3) (2018) 2319–2331. doi:10.1021/acsnano.7b07446.

[44] M. De Santis, A. Buchsbaum, P. Varga, M. Schmid, Growth of ultrathin cobalt oxide films on Pt(111), Physical Review B 84 (12) (2011) 125430. doi:10.1103/PhysRevB.84.125430.

[45] R. Decker, M. Bazarnik, N. Atodiresei, V. Caciuc, S. Blügel, R. Wiesendanger, Local tunnel magnetoresistance of an iron intercalated graphene-based heterostructure, Journal of Physics: Condensed Matter 26 (39) (2014) 394004. doi:10.1088/0953-8984/26/39/394004.

[46] P. Echenique, J. Pendry, Theory of image states at metal surfaces, Progress in Surface Science 32 (2) (1989) 111–159. doi:10.1016/0079-6816(89)90015-4.

[47] T. Filleter, K. V. Emtsev, Th. Seyller, R. Bennewitz, Local work function measurements of epitaxial graphene, Applied Physics Letters 93 (13) (2008) 133117. doi:10.1063/1.2993341.

[48] W. M. C. Foulkes, R. Haydock, Tight-binding models and density-functional theory, Physical Review B 39 (17) (1989) 12520–12536. doi:10.1103/PhysRevB.39.12520.

[49] T. Gao, Y. Gao, C. Chang, Y. Chen, M. Liu, S. Xie, K. He, X. Ma, Y. Zhang, Z. Liu, Atomic-Scale Morphology and Electronic Structure of Manganese Atomic Layers Underneath Epitaxial Graphene on SiC(0001), ACS Nano 6 (8) (2012) 6562–6568. doi:10.1021/nn302303n.

[50] G. Giovannetti, P. A. Khomyakov, G. Brocks, V. M. Karpan, J. van den Brink, P. J. Kelly, Doping Graphene with Metal Contacts, Physical Review Letters 101 (2) (2008) 026803. doi:10.1103/PhysRevLett.101.026803.

[51] D. Gugel, D. Niesner, C. Eickhoff, S. Wagner, M. Weinelt, T. Fauster, Two-photon photoemission from image-potential states of epitaxial graphene, 2D Materials 2 (4) (2015) 045001. doi:10.1088/2053-1583/2/4/045001.

[52] N. P. Guisinger, G. M. Rutter, J. N. Crain, C. Heiliger, P. N. First, J. A. Stroscio, Atomic-scale investigation of graphene formation on 6H-SiC(0001), Journal of Vacuum Science & Technology A: Vacuum, Surfaces, and Films 26 (4) (2008) 932. doi:10.1116/1.2900661.

[53] J. Harris, Simplified method for calculating the energy of weakly interacting fragments, Physical Review B 31 (4) (1985) 1770–1779. doi:10.1103/PhysRevB.31.1770.

[54] J. Hass, F. Varchon, J. E. Millán-Otoya, M. Sprinkle, N. Sharma, W. A. de Heer, C. Berger, P. N. First, L. Magaud, E. H. Conrad, Why Multilayer Graphene on 4H-SiC(000-1) Behaves Like a Single Sheet of Graphene, Physical Review Letters 100 (12) (2008) 125504. doi:10.1103/PhysRevLett.100.125504.

[55] I. Horcas, R. Fernández, J. M. Gómez-Rodríguez, J. Colchero, J. Gómez-Herrero, A. M. Baro, WSXM: A software for scanning probe microscopy and a tool for nanotechnology, Review of Scientific Instruments 78 (1) (2007) 013705. doi:10.1063/1.2432410.

[56] Z. Huang, Z. Xu, J. Zhou, H. Chen, W. Rong, Y. Lin, X. Wen, H. Zhu, K. Wu, Local Work Function Measurements of Thin Oxide Films on Metal Substrates, The Journal of Physical Chemistry C 123 (29) (2019) 17823–17828. doi:10.1021/acs.jpcc.9b03253.

[57] H. Kawano, Effective Work Functions of the Elements, Progress in Surface Science 97 (1) (2022) 100583. doi:10.1016/j.progsurf.2020.100583.

[58] P. A. Khomyakov, G. Giovannetti, P. C. Rusu, G. Brocks, J. van den Brink, P. J. Kelly, First-principles study of the interaction and charge transfer between graphene and metals, Physical Review B 79 (19) (2009) 195425. doi:10.1103/PhysRevB.79.195425.

[59] O.Yu. Kolesnychenko, Yu.A. Kolesnichenko, O. Shklyarevskii, H. van Kempen, Field-emission resonance measurements with mechanically controlled break junctions, Physica B: Condensed Matter 291 (3-4) (2000) 246–255. doi:10.1016/S0921-4526(99)02884-7.

[60] S. Kovalenko, B. Andryushechkin, K. Eltsov, STM study of oxygen intercalation at the graphene/Ni(111) interface, Carbon 164 (2020) 198–206. doi:10.1016/j.carbon.2020.03.054.

[61] J. A. Kubby, Y. R. Wang, W. J. Greene, Electron interferometry at a heterojunction interface, Physical Review Letters 65 (17) (1990) 2165–2168. doi:10.1103/PhysRevLett.65.2165.

[62] P. Lauffer, K. V. Emtsev, R. Graupner, Th. Seyller, L. Ley, S. A. Reshanov, H. B. Weber, Atomic and electronic structure of few-layer graphene on SiC(0001) studied with scanning tunneling microscopy and spectroscopy, Physical Review B 77 (15) (2008) 155426. doi:10.1103/PhysRevB.77.155426.

[63] J. P. Lewis, P. Jelínek, J. Ortega, A. A. Demkov, D. G. Trabada, B. Haycock, H. Wang, G. Adams, J. K. Tomfohr, E. Abad, H. Wang, D. A. Drabold, Advances and applications in the FIREBALL ab initio tight-binding molecular-dynamics formalism, Physica Status Solidi B 248 (9) (2011) 1989–2007. doi:10.1002/pssb.201147259.

[64] Q. Liao, H. J. Zhang, K. Wu, H. Y. Li, S. N. Bao, P. He, Intercalation of cobalt underneath a monolayer of graphene on Ru(0001), Surface Review and Letters 19 (04) (2012) 1250041. doi:10.1142/S0218625X12500412.

[65] C. L. Lin, S. M. Lu, W. B. Su, H. T. Shih, B. F. Wu, Y. D. Yao, C. S. Chang, T. T. Tsong, Manifestation of Work Function Difference in High Order Gundlach Oscillation, Physical Review Letters 99 (21) (2007) 216103. doi:10.1103/PhysRevLett.99.216103.

[66] S.-M. Lu, W.-Y. Chan, W.-B. Su, W. W. Pai, H.-L. Liu, C.-S. Chang, Characterization of external potential for field emission resonances and its applications on nanometer-scale measurements, New Journal of Physics 20 (4) (2018) 043014. doi:10.1088/1367-2630/aab5c7.

[67] X. Luo, G. Liang, X. Sun, Y. Li, F. Yu, L. Wei, X. Cheng, L. Sun, X. Zhao, Charge-neutral epitaxial graphene on 6H–SiC(0001) via FeSi intercalation, Carbon 156 (2020) 187–193. doi:10.1016/j.carbon.2019.09.061.

[68] P. Mallet, F. Varchon, C. Naud, L. Magaud, C. Berger, J.-Y. Veuillen, Electron states of mono- and bilayer graphene on SiC probed by scanning-tunneling microscopy, Physical Review B 76 (4) (2007) 041403. doi:10.1103/PhysRevB.76.041403.

[69] S. Mammadov, J. Ristein, J. Krone, C. Raidel, M. Wanke, V. Wiesmann, F. Speck, T. Seyller, Work function of graphene multilayers on SiC(0001), 2D Materials 4 (1) (2017) 015043. doi:10.1088/2053-1583/4/1/015043.

[70] L. Muehlhoff, W. J. Choyke, M. J. Bozack, J. T. Yates, Comparative electron spectroscopic studies of surface segregation on SiC(0001) and SiC(000$\bar{1}$), Journal of Applied Physics 60 (8) (1986) 2842–2853. doi:10.1063/1.337068.

[71] Y. Murata, V. Petrova, B. B. Kappes, A. Ebnonnasir, I. Petrov, Y.-H. Xie, C. V. Ciobanu, S. Kodambaka, Moiré Superstructures of Graphene on Faceted Nickel Islands, ACS Nano 4 (11) (2010) 6509–6514. doi:10.1021/nn102446y.

[72] D. Pierucci, H. Sediri, M. Hajlaoui, E. Velez-Fort, Y. J. Dappe, M. G. Silly, R. Belkhou, A. Shukla, F. Sirotti, N. Gogneau, A. Ouerghi, Self-organized metal-semiconductor epitaxial graphene layer on off-axis 4H-SiC(0001), Nano Research 8 (3) (2015) 1026–1037. doi:10.1007/s12274-014-0584-y.

[73] K. Rahnejat, C. Howard, N. Shuttleworth, S. Schofield, K. Iwaya, C. Hirjibehedin, Ch. Renner, G. Aeppli, M. Ellerby, Charge density waves in the graphene sheets of the superconductor CaC6, Nature Communications 2 (1) (2011) 558. doi:10.1038/ncomms1574.

[74] S. Rajput, Y. Y. Li, L. Li, Direct experimental evidence for the reversal of carrier type upon hydrogen intercalation in epitaxial graphene/SiC(0001), Applied Physics Letters 104 (4) (2014) 041908. doi:10.1063/1.4863469.

[75] A. Sandin, A. Pronschinske, J. E. J. Rowe, D. B. Dougherty, Incomplete screening by epitaxial graphene on the Si face of 6H–SiC(0001), Applied Physics Letters 97 (11) (2010) 113104. doi:10.1063/1.3484966.

[76] V. M. Silkin, J. Zhao, F. Guinea, E. V. Chulkov, P. M. Echenique, H. Petek, Image potential states in graphene, Physical Review B 80 (2009) 4.

[77] V. M. Silkin, E. Kogan, G. Gumbs, Screening in Graphene: Response to External Static Electric Field and an Image-Potential Problem, Nanomaterials 11 (6) (2021) 1561. doi:10.3390/nano11061561.

[78] U. Starke, C. Riedl, Epitaxial graphene on SiC(0001) and SiC(000^{-}1): from surface reconstructions to carbon electronics, Journal of Physics: Condensed Matter 21 (13) (2009) 134016. doi:10.1088/0953-8984/21/13/134016.

[79] S. Stuckenholz, C. Büchner, M. Heyde, H.-J. Freund, MgO on Mo(001): Local Work Function Measurements above Pristine Terrace and Line Defect Sites, The Journal of Physical Chemistry C 119 (22) (2015) 12283–12290. doi:10.1021/jp512575n.

[80] W. B. Su, S. M. Lu, H. T. Shih, C. L. Jiang, C. S. Chang, T. T. Tsong, Manifestation of the quantum size effect in transmission resonance, Journal of Physics: Condensed Matter 18 (27) (2006) 6299–6305. doi:10.1088/0953-8984/18/27/013.

[81] R. M. Tromp, J. B. Hannon, Thermodynamics and Kinetics of Graphene Growth on SiC(0001), Physical Review Letters 102 (10) (2009) 106104. doi:10.1103/PhysRevLett.102.106104.

[82] T. Vaara, J. Vaari, J. Lahtinen, Adsorption of Potassium on Co(0001), Surface Science 395 (1) (1998) 88–97. doi:10.1016/S0039-6028(97)00618-3.

[83] C. van Efferen, J. Berges, J. Hall, E. van Loon, S. Kraus, A. Schobert, T. Wekking, F. Huttmann, E. Plaar, N. Rothenbach, K. Ollefs, L. M. Arruda, N. Brookes, G. Schönhoff, K. Kummer, H. Wende, T. Wehling, T. Michely, A full gap above the Fermi level: the charge density wave of monolayer VS2, Nature Communications 12 (1) (2021) 6837. doi:10.1038/s41467-021-27094-x.

[84] A. A. Villaeys, Y. J. Dappe, F. P. Lohner, Dynamics of the image surface state in two-photon photoemission spectroscopy, Physical Review B 63 (15) (2001) 155113. doi:10.1103/PhysRevB.63.155113.

[85] B. Wang, M. Caffio, C. Bromley, H. Früchtl, R. Schaub, Coupling Epitaxy, Chemical Bonding, and Work Function at the Local Scale in Transition Metal-Supported Graphene, ACS Nano 4 (10) (2010) 5773–5782. doi:10.1021/nn101520k.

[86] T. O. Wehling, I. Grigorenko, A. I. Lichtenstein, A. V. Balatsky, Phonon-Mediated Tunneling into Graphene, Physical Review Letters 101 (21) (2008) 216803. doi:10.1103/PhysRevLett.101.216803.

[87] J. Wintterlin, M. L. Bocquet, Graphene on metal surfaces, Surface Science 603 (10) (2009) 1841–1852. doi:10.1016/j.susc.2008.08.037.

[88] A. Yurtsever, J. Onoda, T. Iimori, K. Niki, T. Miyamachi, M. Abe, S. Mizuno, S. Tanaka, F. Komori, Y. Sugimoto, Effects of Pb Intercalation on the Structural and Electronic Properties of Epitaxial Graphene on SiC, Small 12 (29) (2016) 3956–3966. doi:10.1002/smll.201600666.

[89] Q. Zhang, J. Yu, P. Ebert, C. Zhang, C.-R. Pan, M.-Y. Chou, C.-K. Shih, C. Zeng, S. Yuan, Tuning Band Gap and Work Function Modulations in Monolayer hBN/Cu(111) Heterostructures with Moiré Patterns, ACS Nano 12 (9) (2018) 9355–9362. doi:10.1021/acsnano.8b04444.